International Journal of Solids and Structures 51 (2014) 4176–4187

Contents lists available at ScienceDirect

International Journal of Solids and Structures

journal homepage: www.elsevier.com/locate/ijsolstr

Cracking mechanisms in lithiated silicon thin film electrodes

Huck Beng Chew [a,*], Binyue Hou [a], Xueju Wang [b], Shuman Xia [b]

[a] Department of Aerospace Engineering, University of Illinois at Urbana-Champaign, Urbana, IL, USA
[b] Woodruff School of Mechanical Engineering, Georgia Institute of Technology, Atlanta, GA, USA

ARTICLE INFO

Article history:
Received 6 March 2014
Received in revised form 7 August 2014
Available online 23 August 2014

Keywords:
Lithium ion battery
Lithiation-induced stress
Sequential cracking
Silicon islands
Finite element analysis

ABSTRACT

The massive cracking of silicon thin film electrodes in lithium ion batteries is associated with the colossal volume changes that occur during lithiation and delithiation cycles. However, the underlying cracking mechanism or even whether fracture initiates during lithiation or delithiation is still unknown. Here, we model the stress generation in amorphous silicon thin films during lithium insertion, fully accounting for the effects of finite strains, plastic flow, and pressure-gradients on the diffusion of lithium. Our finite element analyses demonstrate that the fracture of lithiated silicon films occurs by a sequential cracking mechanism which is distinct from fracture induced by residual tension in conventional thin films. During early-stage lithiation, the expansion of the lithium-silicon subsurface layer bends the film near the edges, and generates a high tensile stress zone at a critical distance away within the lithium-free silicon. Fracture initiates at this high tension zone and creates new film edges, which in turn bend and generate high tensile stresses a further critical distance away. Under repeated lithiation and delithiation cycles, this sequential cracking mechanism creates silicon islands of uniform diameter, which scales with the film thickness. The predicted island sizes, as well as the abrupt mitigation of fracture below a critical film thickness due to the diminishing tensile stress zone, is quantitatively in good agreement with experiments.

1. Introduction

Lithium ion batteries are high energy density systems that store energy by insertion of lithium ions into solid electrodes. Silicon is one of the most promising electrode materials for high performance lithium ion batteries, since it possesses the highest known specific capacity of 4200 mAh/g, which is an order of magnitude higher than conventional graphite electrodes. During lithiation, the silicon electrodes form Li_xSi compounds, and undergo huge volume expansion of about 300% since one silicon atom can theoretically bond with a maximum of $x = 3.75$ lithium atoms. This huge volume change during cycles of lithiation and delithiation leads to massive cracking of the electrodes, and subsequent loss in capacity (Beaulieu et al., 2001). However, studies have shown that silicon electrodes of small feature sizes, such as nanowires, nanoparticles, porous structures, and thin films display significantly higher reversible charge capacity and longer cycle life (Lee et al., 2012; Liu et al., 2011; Takamura et al., 2004; Graetz et al., 2003). In fact, a critical feature size of these nanostructured silicon electrodes exists, below which fracture would be completely mitigated. It is believed that the improved fracture resistance originates from the ability of the nanoscale structure to accommodate the lithiation-induced strain by plastic deformation, resulting in lower stresses present during volume changes (Sethuraman et al., 2010; Zhao et al., 2011). However, the circumstances leading to the size-dependent fracture of these nanostructured silicon electrodes are still not well understood.

Silicon thin films are a particularly useful model system to study the size-dependent fracture of silicon electrodes during lithiation and delithiation cycles. Li et al. (2011) examined the cracking patterns generated during electrochemical cycling of amorphous silicon thin film electrodes, and found that decreasing film thickness significantly increased the density of cracks, resulting in island diameters that are smaller but nearly uniform (Fig. 1). Once formed, the individual silicon islands remain crack-free under subsequent lithiation and delithiation cycles. This suggests that a critical island diameter exists for a fixed film thickness, below which fracture of the electrode would be mitigated. In addition, studies show that a critical silicon film thickness also exists, below which a continuous film no longer cracks even under repeated cycling (Li et al., 2011; Takamura et al., 2004). These observations demonstrate that the cracking of the silicon thin film electrode, resulting in mechanical degradation and capacity loss, may be

* Corresponding author. Tel.: +1 217 333 9770.
E-mail address: hbchew@illinois.edu (H.B. Chew).

http://dx.doi.org/10.1016/j.ijsolstr.2014.08.008
0020-7683/

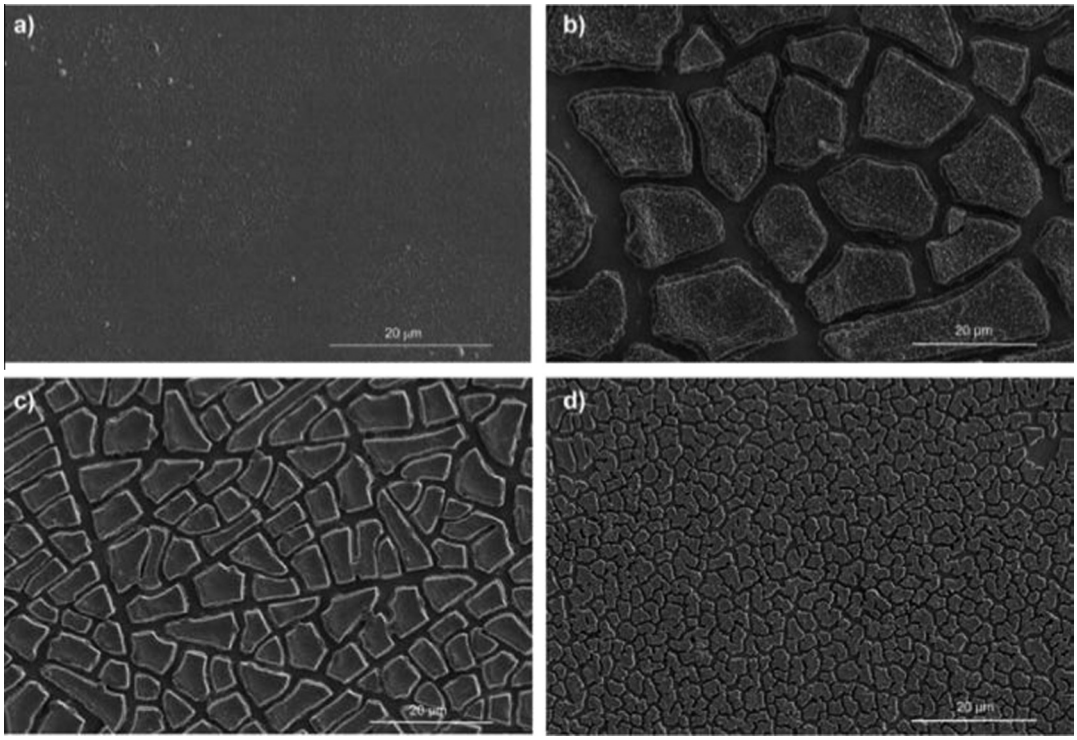

Fig. 1. Scanning electron microscopy (SEM) images of crack patterns formed on amorphous silicon (a-Si) thin films (Li et al., 2011). (a) 500 nm thick a-Si film before electrochemical tests. (b) 1000 nm thick, after 5 cycles. (c) 500 nm thick, after 5 cycles. (d) 200 nm thick, after 10 cycles.

alleviated by controlling the film thickness and through patterning of silicon islands on a substrate.

The crack patterns that form in silicon thin film electrodes during lithiation and delithiation cycles closely resemble through-thickness crack networks that form in drying media and thin films with residual tensile stress, leading many to conclude that the fracture of the silicon electrodes occurs during the delithiation cycle (Xiao et al., 2011; Li et al., 2011; Beaulieu et al., 2001). Moreover, experimental measurements show that the curvature-induced average stress of the silicon film is always in compression during lithiation and in tension during delithiation (Sethuraman et al., 2010). The common explanation is that the expansion of the silicon thin film during insertion of lithium is constrained by the underlying substrate, which compresses the silicon film and plastically deforms the substrate. During the removal of lithium ions, the residual plastic deformation in the substrate will induce tensile stress in the silicon film. Under repeated volumetric cycling of the silicon thin film electrodes, a plastic ratcheting mechanism occurs causing massive cracking of the silicon electrodes (Maranchi et al., 2006). This explanation, while plausible, fails to account for the order-of-magnitude differences in crack spacing (island size) predicted by conventional theories of thin film fracture. In conventional engineering films and coatings under residual tension, the crack spacing is of the same order as the film thickness, except when the film is much stiffer than the substrate (Ye et al., 1992; Xia and Hutchinson, 2000; Huang et al., 2003). Cracks in mud-flats – a common analogy to describe the crack patterns in lithium-silicon films (Beaulieu et al., 2001) – also display an average spacing comparable to their depth (Goehring et al., 2010). However, the average crack spacings in lithiated silicon films of 200–1000 nm thick are an order of magnitude larger, and range from 2 μm to 10 μm (Moon et al., 2006; Maranchi et al., 2006; Li et al., 2011). This discrepancy suggests that the cracking mechanism of lithiated silicon films could be very different from the previously assumed mechanism of fracture induced by residual tension akin to conventional thin films. Xiao et al. (2011) put forth a possible mechanism to account for the cracking patterns by including the effects of interface slip on the critical crack spacing required to induce strain localization in the lithiated film. However, their theoretical explanation was based on a highly idealized case of uniform residual tension induced in the film during delithiation, and neglects the effects of stress-gradients which develop during lithiation or delithiation processes.

Recent experiments have shown that cracking of crystalline silicon nanowires, nanopillars, and nanospheres occur during the lithiation cycle (Ryu et al., 2011; Lee et al., 2012; Huang et al., 2013). In the case of silicon nanopillars, the fracture locations are found to be strongly anisotropic, and correlated with anisotropic expansion of these nanostructures (Lee et al., 2012). In nanospheres, a proposed explanation is that the external curved surface of the lithiated silicon is subjected to tensile hoop stress during lithiation, leading to fracture (Huang et al., 2013). Numerical predictions also point to the possibility of high tensile stresses developing within the core of these structures during lithiation (Ryu et al., 2011). Contrary to previous explanations of silicon thin film fracture under delithiation, we instead show that cracking of an initially flat amorphous isotropic thin film also occurs during the lithiation cycle. Our finite element simulations predict that the cracking occurs sequentially, initiating near the film edges during early-stage lithiation, and progressing towards the center of the film under repeated lithiation and delithiation cycles. The critical silicon island sizes and critical film thickness for mitigation of fracture predicted by our numerical model are quantitatively in close agreement with experiments.

2. Problem formulation

2.1. Coupled lithiation and deformation

Our numerical model for the fully coupled large deformation and lithium diffusion problem follows previously developed

frameworks (Bower et al., 2011; Zhao et al., 2011). We introduce the unstressed configuration of the silicon thin film with zero concentration of lithium as the reference configuration for describing shape change and transport. The change in shape of infinitesimal volume elements within the solid can be characterized by the deformation gradient in standard finite deformation notation as $F_{ij} = dx_i/dX_j$, where x_i and X_i are coordinates of a material point in the deformed and undeformed configurations respectively. We separate the total deformation F_{ij} into contributions from the elastic distortion of the lattice, expansion due to lithium ion insertion, and plastic flow resulting in shape change:

$$F_{ij} = F^e_{ik} F^c_{kl} F^p_{lj} \tag{1}$$

The elasto-plastic portion of the deformation, i.e. F^e_{ij} and F^p_{ij}, follows the standard framework of finite deformation elasticity and plasticity. Since our silicon thin film electrode is amorphous, we assume that the volume expansion of the material element caused by lithium insertion with respect to the volume of lithium-free silicon Λ occurs isotropically

$$F^c_{ij} = \mathbf{I} + \sqrt[3]{\Lambda}\delta_{ij} \tag{2}$$

where $\mathbf{I}$ is the identity matrix. Treating the volume expansion per mole of lithium ion insertion Ω as a constant,

$$\Lambda = \Omega \mathrm{C} \tag{3}$$

where C is the nominal concentration given by the number of moles of lithium ions per unit volume of the lithium-free silicon. When the silicon film is fully-lithiated, the compound $Li_{15}Si_4$ forms. Then, each mole of silicon contains 3.75 mol of lithium, and the volume of the lithiated silicon expands by 300%. Assuming that pure amorphous silicon has a molar density of $\rho_0 = 7.874 \times 10^4$ mol/m^3 (Mohr et al., 2008), and substituting $\Lambda = 3$ with $\mathrm{C} = 3.75\rho_0$ in (3), we obtain $\Omega = 1.016 \times 10^{-5}$ m^3/mol.

The chemical potential of lithium in the material element can be expressed as (Bower et al., 2011; Zhao et al., 2011)

$$\mu = \mu_0 + AkT \ln(\mathrm{c}) - \Omega\sigma_m \tag{4}$$

where μ_0 is a reference value, A is the Avogadro's number, k the Boltzman's constant, T the temperature, and σ_m the mean stress. The true concentration of lithium ions (moles per unit volume in current configuration) is related to the nominal concentration by $\mathrm{c} = \mathrm{C}/\det(F_{ij})$. Then, the true flux of lithium ions is given by

$$j_i = -\frac{cD_0}{kT}\frac{\partial \mu}{\partial x_i} \tag{5}$$

where D_0 is the diffusion constant taken to be 10^{-16} m^2/s (Ding et al., 2009).

2.2. Numerical implementation

To solve this coupled large deformation and lithium diffusion problem, we reformulate the diffusion equation into an *equivalent* heat equation augmented to account for pressure-gradient effects in (5), and perform a coupled thermal-stress analysis using the commercial finite element program, Abaqus 6.11. The temperature change $\Delta\hat{T}$ in the equivalent thermal-stress problem is used to represent the normalized nominal lithium concentration $\bar{\mathrm{C}} = \mathrm{C}/\rho_0$, which ranges from 0 for lithium-free silicon, to 3.75 for fully-lithiated silicon. Then, the stress-free isotropic volume expansion associated with lithium ion insertion with respect to the volume of lithium-free silicon in (3) is treated in the context of volumetric thermal expansion, written as

$$\alpha^v \Delta\hat{T} = \Omega\bar{\mathrm{C}} \tag{6}$$

where α^v is the volumetric thermal expansion coefficient, which is related to the definition of thermal expansion coefficient α by

$$\alpha^v \Delta\hat{T} = 3\alpha\Delta\hat{T} + 3\alpha^2(\Delta\hat{T})^2 + \alpha^3(\Delta\hat{T})^3 \tag{7}$$

This expression is valid for large deformation, i.e. $\Delta\hat{T} \gg 1$, which is necessary to describe the lithiation process, and only reduces to the usual definition of $\alpha^v = 3\alpha$ when the deformation is small. Substituting $\alpha^v = \Omega$ in (7), we obtain $\alpha = 0.157$. With large deformation, an increment of thermal expansion is based on an increment of temperature change and the current dimensions of each element. Our thermal-lithium-concentration equivalence in (6) and (7), however, is formulated based on volume change per unit volume of lithium-free silicon, i.e. α represents the "nominal" thermal expansion coefficient. Knowing that the thermal expansion will be integrated over substeps and that the temperature is ramping up during these substeps, the "true" thermal expansion coefficient $\bar{\alpha}$ will be adjusted accordingly with $\bar{\mathrm{C}}$ as follows

$$\bar{\alpha} = \frac{\ln(\alpha\bar{\mathrm{C}} + 1)}{\bar{\mathrm{C}}} \tag{8}$$

In a thermal heat transfer equation, the heat flux is driven purely by temperature gradients. From (4) and (5), however, diffusion of lithium ions in the material element is driven both by the concentration gradient, as well as the pressure-gradient. We obtain the latter explicitly using a backward scheme. We average the mean stress at the nodes at time step $i-1$, and calculate the gradient of the mean stress at the integration points of each element at step i by taking the derivative of the bilinear shape functions. This pressure-gradient term is then incorporated in the calculation of lithium flux through the user-defined heat transfer subroutine UMATHT in Abaqus.

2.3. Finite element modeling

Our model geometry consists of an amorphous silicon thin film of length d and thickness h attached to a thick copper substrate, as shown in Fig. 2. Due to geometrical symmetry along $x_1 = 0$, we model only one-half of the geometry in the finite element method (FEM) assuming plane strain condition. The silicon film thickness is varied from h = 100 nm to 1000 nm, while the thickness of the copper substrate is fixed at 2.1 μm. Our parametric studies show that this copper substrate thickness is sufficient to represent an infinitely thick substrate. For the purpose of our analysis, we do not make any distinction between a silicon film and a silicon island since both essentially comprise of a thin layer of silicon deposited on a thick copper substrate. The model length d represents the size of the silicon film, and ranges from 1 μm to 40 μm. We note that the stress distributions are self-similar away from the film edges, and the full stress characteristics of actual films which are centimeters in length can be effectively captured with a model length of d = 40 μm. Roller boundary conditions are imposed along the

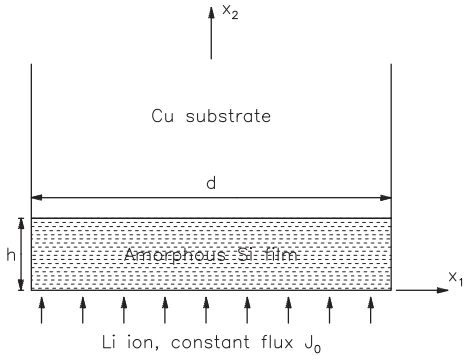

Fig. 2. Schematic of an amorphous silicon film of length d and thickness h deposited on a copper substrate, and subjected to lithiation with constant flux J_0.

plane of symmetry of the film and substrate at $x_1 = 0$, as well as along the end of the copper substrate. The free-surfaces of the film along $x_2 = 0$ and $x_1 = d/2$ are taken to be traction-free. The silicon film is lithiated by prescribing a constant flux J_0 on the surface of the film along $x_2 = 0$. See schematic in Fig. 2. This prescribed flux (in units of normalized concentration per area per second) in-turn defines the maximum time $\tau_{max} = 3.75h/J_0$ required to fully-lithiate the silicon film to its theoretical maximum to form the compound $Li_{15}Si_4$. Unless otherwise stated, we use a flux of $J_0 = 1\ nm^{-2}\ s^{-1}$ to achieve a realistic charging rate of $\tau_{max} = \sim 1$ h for a 1000 nm thick film. Simulations for charging rates of $J_0 = 0.5\ nm^{-2}\ s^{-1}$ and $2\ nm^{-2}\ s^{-1}$ are also conducted to understand the charging rate effects.

The finite element model is discretized into four-node bilinear quadrilateral plane-strain elements. The total number of elements for a fixed d of 4 μm ranges from 14,000 elements for h = 100 nm to 50,000 elements for h = 1000 nm. In all cases, a regular mesh grid with fixed element size L_s of 10 nm by 10 nm is used to model the silicon film. Since the calculation of the pressure-gradient term in (5) is done explicitly, a small time increment of $t < L_s^2/D_0$ must be enforced to ensure convergence. Here, we imposed a fixed time step of t = 0.02 s, which is 50 times smaller than the calculated maximum allowable t of 1 s. We have performed convergence studies, and have found the effects of further mesh and time-step refinements to be negligible.

Both the silicon film and the copper substrate are assumed to be elastically isotropic, with elastic modulus E_f and E_s, and Poisson's ratio υ_f and υ_s. The plastic responses of the silicon film and copper substrate are characterized by a J_2 flow theory, and undergo perfectly plastic yielding at yield strengths of σ_f and σ_s respectively. The elastic modulus for lithium-free amorphous silicon is 100 GPa. Density functional theory (DFT) calculations show that the elastic modulus of silicon varies substantially with the concentration of lithium ions, but the Poisson's ratio remains almost constant (Shenoy et al., 2010). Based on these DFT calculations, we use the relationship $E_f = 100 - 20\bar{C}$ GPa. For simplicity, we assume the remaining material parameters to be independent of the lithium concentration, and adopt the values $E_s = 120$ GPa, $\upsilon_f = 0.26$, $\upsilon_s = 0.37$, $\sigma_f = 2$ GPa, and $\sigma_s = 0.07$ GPa. Recent DFT calculations suggest that the resistance of the copper/silicon interface to shear-slip is a strong function of the lithium concentration in the silicon film in the vicinity of the interface (Stournara et al., 2013). Since our simulations here primarily focus on early-stage lithiation where the extent of lithiation is largely confined to the silicon thin film surface, we assume the interface between copper and silicon to be fully bonded in our lithiation simulations. For the delithiation simulations, we consider both the fully-bonded no-slip case, as well as the case where interface slip is permitted.

3. Tensile stress development in early-stage lithiation

Previous experiments show that the critical silicon island diameter for mitigation of fracture ranges from ~2 μm for a 200 nm thick film, and scales linearly to ~10 μm for a 1000 nm thick film (Li et al., 2011). Here, the model length of the silicon film is fixed at d = 4 μm, and we consider three different film thicknesses of h = 800, 400 and 100 nm. Based on the experimental data, cracking will be mitigated for the h = 800 nm film, and will be on the verge of termination for the h = 400 nm film. For the h = 100 nm film, experiments show that fracture is not observed regardless of the length of the film. Therefore, examining the tensile stress development across these three film thicknesses will provide insights into the size-dependent fracture of lithiated silicon thin films.

Figs. 3–5 show the distributions of the normalized in-plane σ_{11} stress, von Mises effective stress σ_e, and lithium concentration $\bar{C}$ along the center ($x_1 = 0$) of an initially lithium-free silicon film with thicknesses h = 800, 400 and 100 nm. The films are subjected to a constant flux of $J_0 = 1\ nm^{-2}\ s^{-1}$ applied at time $\tau = 0$. For the silicon film with h = 800 nm in Fig. 3, the influx of lithium ions at time $\tau/\tau_{max} = 0.01$ and 0.02 generates a zone of compression emanating ~0.3h from the surface, with the maximum compressive peak reaching the yield strength near the surface of the film. This zone of compression in turn creates a tension stress zone spanning $0.3 < x_2/h < 0.9$ in the lithium-free silicon. Further lithiation shifts the peak tension stress from $x_2/h = 0.45$ at $\tau/\tau_{max} = 0.02$ to $x_2/h = 0.6$ at $\tau/\tau_{max} = 0.04$, and reduces the magnitude of the peak tensile stress at $\tau/\tau_{max} = 0.08$. Comparison between Fig. 3b and c shows that the buildup of plasticity denoted by the region spanning $\sigma_e = \sigma_f$ assuming monotonic loading, correlates directly with the spread of lithium ions operationally defined by $\bar{C} > 0.1$. This spread of lithium ions reduces the magnitude of the tensile σ_{11} stresses, and creates kinks in the σ_{11} distribution curves at $x_2/h = 0.35$ and 0.65 for $\tau/\tau_{max} = 0.04$ and 0.08, respectively. For the silicon film with h = 400 nm in Fig. 4, the influx of lithium ions similarly creates distinct compression and tension zones. However, the maximum tensile σ_{11} stress now resides near the copper/silicon interface and rapidly approaches the yield strength of unlithiated silicon at $\tau/\tau_{max} = 0.04$. At this early-stage lithiation, plasticity and the spread of lithium ions are still confined to within $x_2/h < 0.3$. At $\tau/\tau_{max} = 0.11$, lithium ions have now diffused throughout the entire film (see spread of the plastic zone in

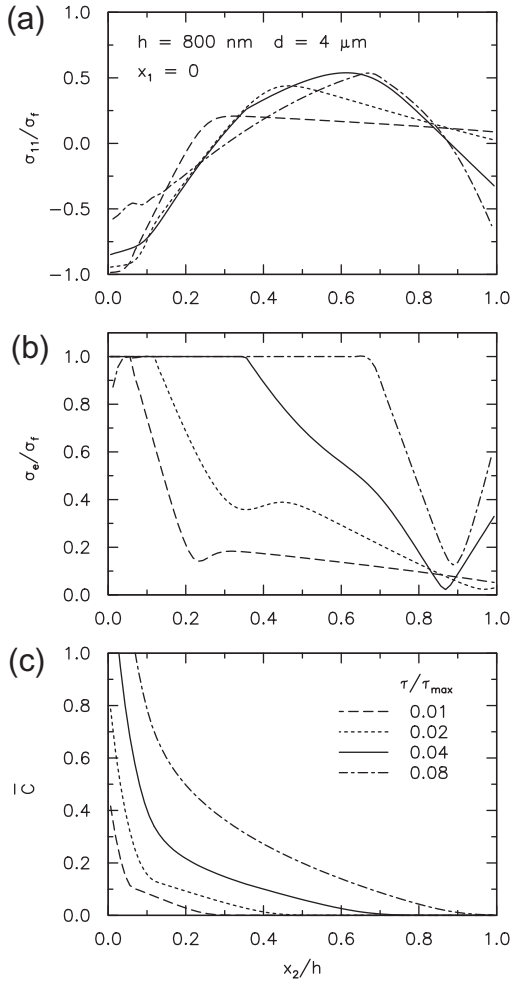

Fig. 3. Distributions of the normalized (a) in-plane σ_{11} stress, (b) von Mises effective stress σ_e, and (c) lithium concentration $\bar{C}$ along the center ($x_1 = 0$) of an initially lithium-free silicon film with thickness h = 800 nm and length d = 4 μm.

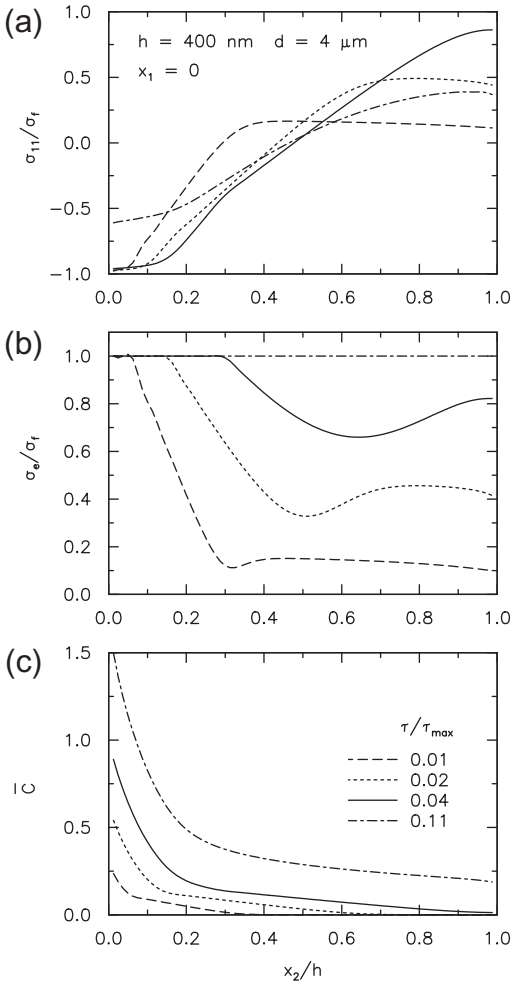

Fig. 4. Distributions of the normalized (a) in-plane σ_{11} stress, (b) von Mises effective stress σ_e, and (c) lithium concentration $\bar{C}$ along the center ($x_1 = 0$) of an initially lithium-free silicon film with thickness h = 400 nm and length d = 4 μm.

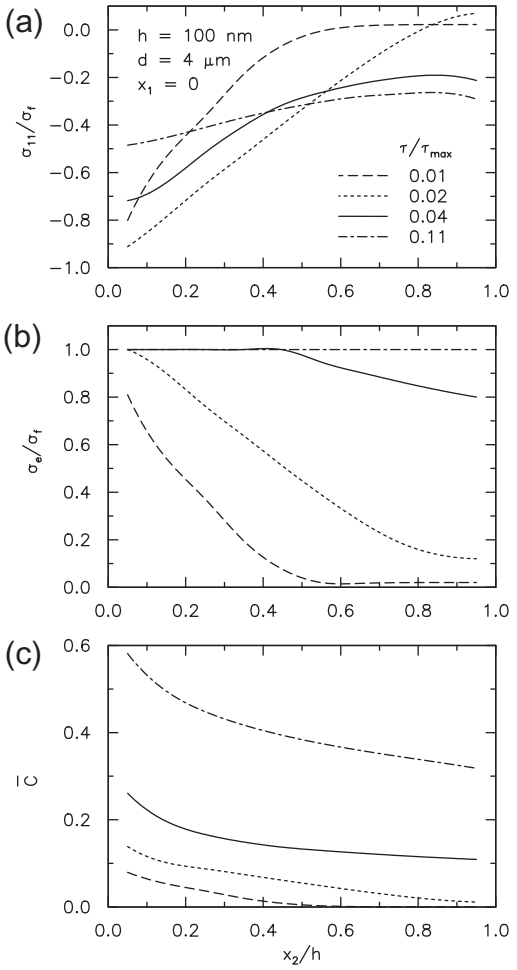

Fig. 5. Distributions of the normalized (a) in-plane σ_{11} stress, (b) von Mises effective stress σ_e, and (c) lithium concentration $\bar{C}$ along the center ($x_1 = 0$) of an initially lithium-free silicon film with thickness h = 100 nm and length d = 4 μm.

Fig. 4b), and the tensile stresses are dramatically reduced. For the silicon film with h = 100 nm in Fig. 5, the entire film undergoes compression even during early-stage lithiation. The film is sufficiently thin that the lithium diffuses throughout the entire film so quickly that tensile σ_{11} stresses in the film cannot build up. See the more uniform $\bar{C}$ for the h = 100 nm film in Fig. 5c, compared to those for h = 800 nm and h = 400 nm films in Fig. 3c and Fig. 4c respectively.

To understand how the tensile σ_{11} stress zone is created by the lithiation process, we examine the evolving σ_{11} stress contours for the h = 400 nm and h = 800 nm films in Figs. 6 and 7. The spread of lithium ions at the different stages, defined by $\sigma_e = \sigma_f$, is shown as dashed lines in the corresponding subplots. For the silicon film with h = 400 nm, the zone of compression during initial lithiation develops concurrently with the spread of lithium ions (Fig. 6a). The expansion associated with further influx of lithium ions bends the film, which relieves some of the compressive σ_{11} stresses near the edge of the film (Fig. 6b). To accommodate the bending caused by outer surface expansion of the lithiated film, high tensile σ_{11} stresses develop at the inner lithium-free zone, reaching a peak near the copper/silicon interface (contours colored in red). As the spread of lithium ion advances towards the interface (Fig. 6c) and approaches the tensile zone, the volume expansion caused by lithiation relaxes the tensile stresses. In fact, the relaxation of both the maximum tensile (red) and compressive (blue) stresses is facilitated by the pressure-gradient term in (5), which accelerates the spread of lithium ions from the high compression zone to the high tension zone. The development of a higher concentration of lithium ions at the high tension zone can be seen from the emergence of a second lithium front from the high tensile stress zone at the copper/silicon interface (Fig. 6c), which eventually joins up with the main lithium front (Fig. 6d). For silicon films with h = 800 nm, the spread of lithium ions similarly creates dual high compression and tension zones (Fig. 7a), but the tensile stress zone residing in the mid-section of the film now has a wider span and is of a lower magnitude. The magnitude of the tensile stresses diminishes with the influx of lithium ions (compare Fig. 7b and c).

We have also conducted simulations for other film thicknesses ranging from h = 100 to 1000 nm. We summarize the σ_{11} contour maps for each h in Fig. 8, taken at the instant when the σ_{11} tensile stress within the silicon film reaches a maximum. For 500 nm $\leqslant h \leqslant$ 1000 nm, the high tensile stress zone resides in the bulk but progressively approaches the copper/silicon interface with decreasing h. For h = 300 nm and 400 nm, the maximum tensile σ_{11} stress now resides near the copper/silicon interface; this shift in the high tensile stress zone from the bulk to the interface is also marked by a significant increase in the magnitude of maximum σ_{11} stress which approaches the yield. This intensification of the σ_{11} stresses for fixed d is attributed to the focusing of the tensile stresses to a narrower zone with decreasing h. For $h \leqslant$ 200 nm, the diminishing tensile stress zone decreases the maximum σ_{11} film stress dramatically.

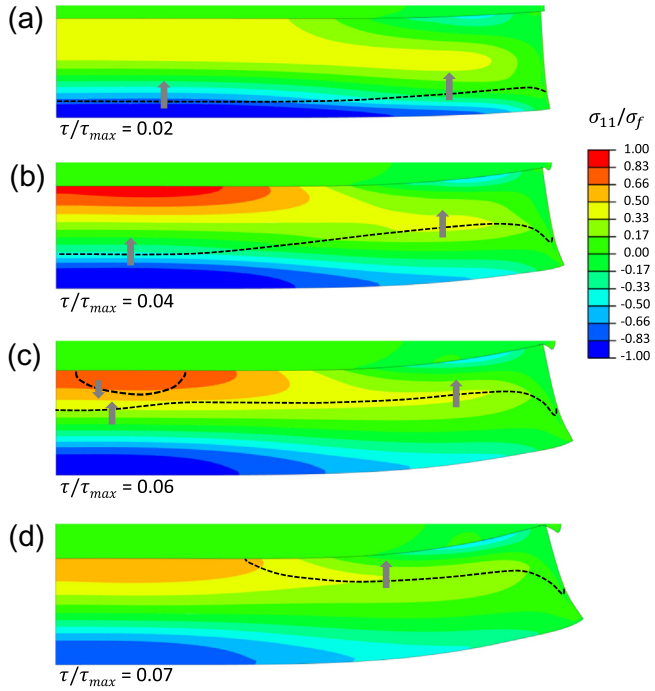

Fig. 6. Evolving σ_{11} stress contours for an initially lithium-free silicon film with h = 400 nm and d = 4 μm. Dashed lines and arrows denote spread of lithium ions defined by $\sigma_e = \sigma_f$.

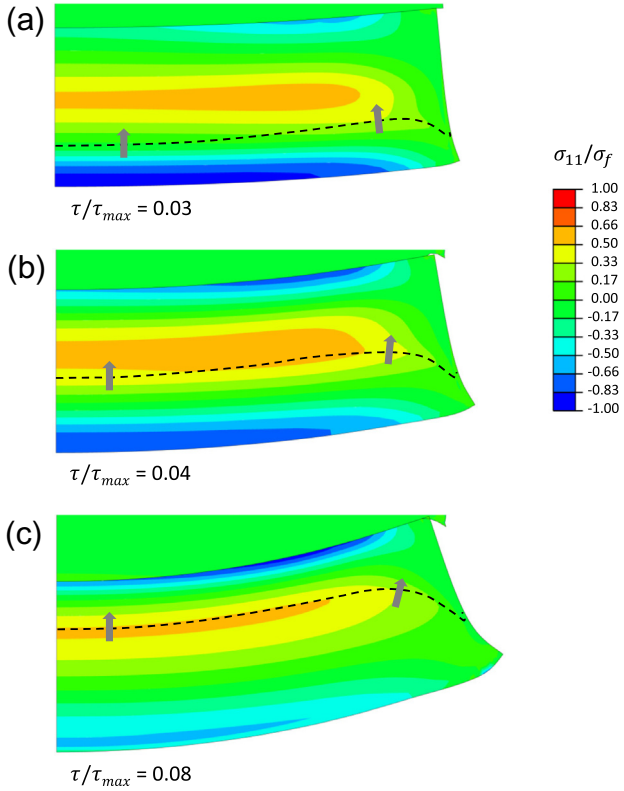

Fig. 7. Evolving σ_{11} stress contours for an initially lithium-free silicon film with h = 800 nm and d = 4 μm. Dashed lines and arrows denote spread of lithium ions defined by $\sigma_e = \sigma_f$.

4. Multiple-island formation mechanism

The development of high σ_{11} stresses during early-stage lithiation of the silicon film is the driving force for fracture. For 600 nm $\leqslant h \leqslant$ 1000 nm in Fig. 8, the maximum tensile stress of ~1.3 GPa (compared to the yield strength of 2 GPa) resides within the bulk of the lithium-free silicon film and is unlikely to initiate fracture propagation. We therefore expect the silicon island size for films with 600 nm $\leqslant h \leqslant$ 1000 nm to remain unchanged at d = 4 μm during subsequent lithiation and delithiation cycles. Likewise for silicon films with $h \leqslant$ 200 nm, the diffusion of lithium ions throughout the entire film prevents high tensile stresses from developing, which will mitigate fracture. For the h = 300–500 nm films, the maximum σ_{11} stress now resides near the silicon/copper interface, and has a higher magnitude of ~1.5–1.8 GPa which is comparable to the yield strength of 2 GPa; this high tension zone can potentially case pre-existing or newly-nucleated flaws to grow. To ascertain this, one requires prior knowledge of both the fracture toughness of the film Γ, as well as its characteristic flaw size a_c.

While lithiated silicon is reported to undergo significant plastic flow, bulk amorphous silicon is extremely brittle under tension and hence plastic flow will be limited to the crack-tip (Zhao et al., 2011). Since the maximum tensile σ_{11} stress resides within the lithium-free silicon near the copper/silicon interface, Γ should be the fracture toughness of amorphous silicon which has a reported value ranging from 3 – 9J/m^2 (Chasiotis et al., 2005; Ballarini et al., 2001, 1997; Chen et al., 1982). The characteristic flaw size created during sputter deposition of thin silicon films on copper substrates is unknown, which has motivated some studies to introduce imperfections of predetermined sizes in the silicon film to facilitate the measurement of the fracture energy (Pharr et al., 2013). However, massive cracking of silicon thin film of thickness greater than 100 nm and silicon nanoparticles of diameter larger than 150 nm has been reported (Li et al., 2011; Takamura et al., 2004; Liu et al., 2012), which suggests that the size of the initial flaws could be a significant fraction of these film thicknesses and particle diameters. As such, the presence of these flaws could considerably perturb the stress field within the film.

To clarify these points, we have introduced perpendicular edge-type cracks originating at the silicon/copper interface, and located where the maximum σ_{11} tensile stress was detected for the pristine silicon film. We subject these crack configurations to the same lithiation process outlined in Section 2. Fig. 9 shows the contour maps of the σ_{11} stresses for h = 300 nm and h = 400 nm silicon films with assumed initial flaw sizes of a_c = 30, 60, and 100 nm; for comparison purposes, the set of contour maps for the respective film thicknesses are taken at the same τ/τ_{max} lithiation instant at which the σ_{11} tensile stress near the silicon/copper interface for a_c = 30 nm reaches a maximum. We note that for both the h = 300 nm and h = 400 nm silicon films, the lithiation time period for these crack-configurations to achieve maximum σ_{11} tensile stress is almost the same as that for the pristine film, and occurs during early-stage lithiation. While the presence of these initial cracks causes some local unloading, the contour stress maps exhibit very similar features to those displayed by the pristine film: high tensile stresses still reside in the vicinity of the silicon/copper interface. The presence of these initial cracks, however, permits bending of the inner pre-cracked section of the film, which exacerbates the tensile stress field directly ahead of the crack-tip.

We quantify the driving force for fracture by calculating the J-integral about a closed-contour surrounding the crack-tip which encompasses the crack-tip plastic zone. Our simulations show that plastic yielding at the crack-tip is confined to a narrow ~30 nm zone, which assures that small-scale yielding conditions are valid. For the (a) h = 300 nm and (b) h = 400 nm films with a_c = 30, 60, and 100 nm, we obtain the J-integral values of (a) 8.1, 15.4, and 24.8 J/m^2, and (b) 8.6, 17.7, and 28.0 J/m^2, respectively. Since the driving force for crack propagation in the silicon film lies either at the upper-bound (for a_c = 30 nm) or exceeds the

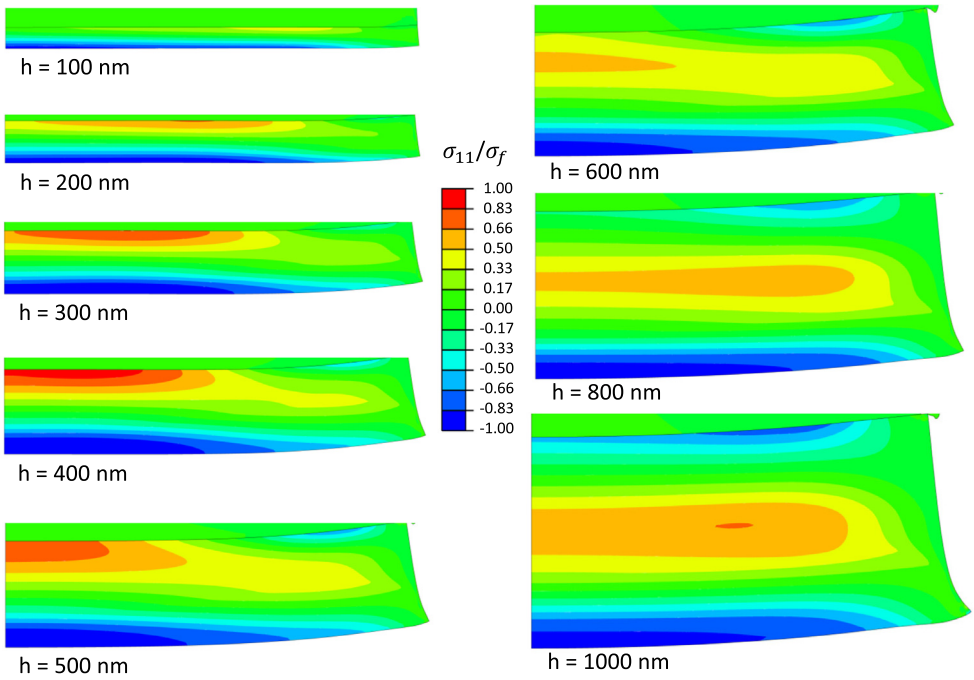

Fig. 8. Contour maps of σ_{11} stresses taken at the instant when the σ_{11} tensile stress within the silicon film reaches a maximum, for film thicknesses ranging from h = 100 to 1000 nm, with d = 4 μm.

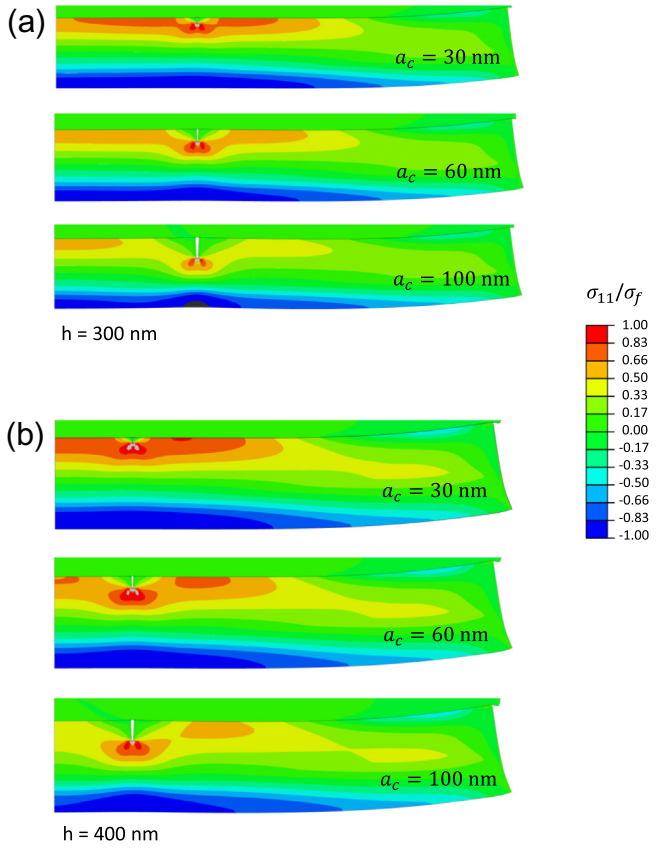

Fig. 9. Contour maps of σ_{11} stresses for crack configurations of a_c = 30, 60, and 100 nm for (a) h = 300 nm and (b) h = 400 nm with d = 4 μm, taken at the same lithiation instant when the σ_{11} tensile stress within the silicon film with a_c = 30 nm reaches a maximum.

experimentally-measured fracture toughness of amorphous silicon films (for a_c = 60, 100 nm), we can therefore conclude that cracks will indeed grow for both the h = 300 nm and h = 400 nm films with initial flaws of a_c = 30 nm or larger. Similar trends are observed for the h = 500 nm film. In addition, consistently larger K-fields are experienced by cracks with larger a_c at the same loading instant, particularly since the presence of these larger cracks facilitates the bending of this inner cracked-section of the film. This implies that once the driving force for fracture exceeds Γ, the crack will unstably propagate towards the surface. However, the crack will be arrested at the high compression zone within the subsurface of the lithiated-silicon film, which explains why internal cracks are not observed during the lithiation process (Li et al., 2011).

In all our simulations above, we have kept the horizontal dimensions of the film and substrate fixed at d = 4 μm. Fig. 10 compares the σ_{11} stress contours for pristine silicon islands with fixed film thickness of h = 400 nm, and with island sizes d ranging from 1 μm to 40 μm. During early stage lithiation, the diffusion of lithium in the silicon film creates a lithiated-silicon subsurface layer which expands volumetrically. This subsurface expansion bends the film near the edges, and relieves much of the compressive stress there. For 1 μm $\leqslant d \leqslant$ 3 μm, the entire silicon island is subjected to bending, and large compression surface stresses or bulk tensile stresses cannot build-up. Fracture of islands with $d \leqslant$ 3 μm is therefore not possible. For 4 μm $\leqslant d \leqslant$ 40 μm, the subsurface lithiated-silicon layer undergoes large compressive σ_{11} stresses some critical distance d_c away from the edges, which in turn generates high tensile σ_{11} stresses within a narrow zone near the silicon/copper interface. As demonstrated in our fracture analysis above, these high tensile σ_{11} stresses are sufficient to nucleate cracks to cause fracture. Close examination shows that the maximum σ_{11} stresses for all $d \geqslant$ 4 μm are approximately of the same magnitude, reaching the ~2 GPa yield strength, and are located at the same fixed distance of $d_c \sim$ 2 μm from the film edge. For all $d \geqslant$ 4 μm, the high tensile stress zone defined by $\sigma_{11} > 0.75\sigma_f$ spans a width of ~1 μm in the x_1 direction, which suggests that the nucleation of a single finite crack within this zone will be sufficient to relax the tensile stresses. Away from this tensile stress zone closer to the mid-span (x_1 = 0), the edge effect diminishes; the lithiation-induced deformation is now accommodated by both the film and

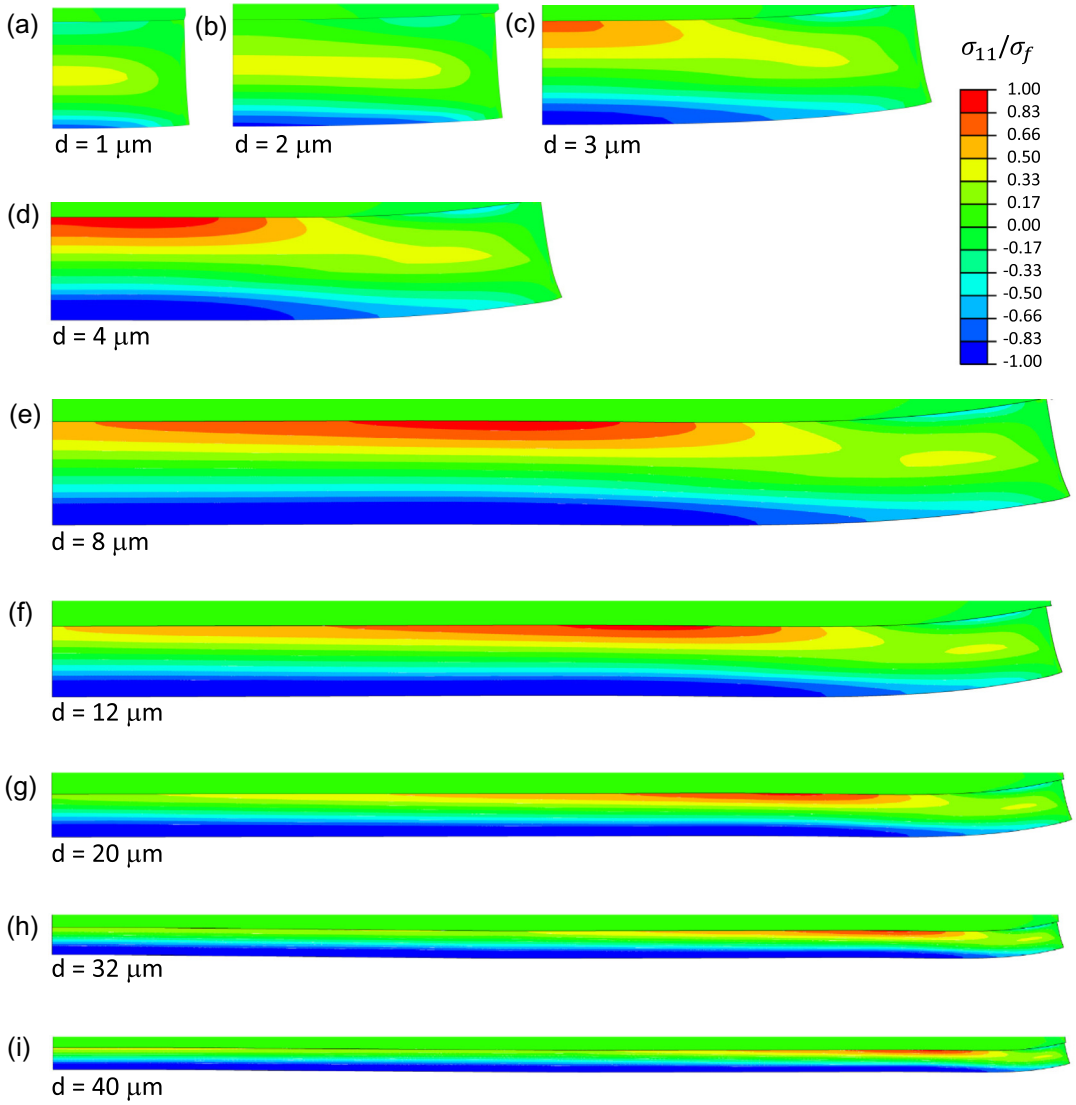

Fig. 10. Contour maps of σ_{11} stresses taken at the instant when the σ_{11} tensile stress within the silicon film reaches a maximum, for fixed film thickness of h = 400 nm, with d ranging from 1 μm to 40 μm. Contour maps for (f)–(i) are not of the same scale.

the substrate, resulting in low tensile σ_{11} stress buildup in the lithium-free silicon. We have repeated the calculations for silicon islands with fixed film thickness of h = 800 nm in Fig. 11 and have obtained similar trends. The maximum σ_{11} stress is now located at a critical distance $d_c \sim 3.5$ μm from the edges, which remains independent of d; high tensile σ_{11} stresses are not observed for island sizes of $d = 6$ μm and below.

The above mechanism of bending-induced crack nucleation near the film edges is summarized in Fig. 12a. The initiation of fracture at the film edges suggests that the massive cracking of silicon thin film electrodes occurs by a sequential island-to-island formation mechanism during early-stage lithiation. For a film size of $d \gg 2d_c$, the nucleation of perpendicular micro-cracks to the silicon/copper interface at the distance d_c from the film edges alleviates the high tensile σ_{11} stresses there. At the new crack site, the newly-formed free-surfaces now allow the inner sections of the film to bend. Unlike the constraint-free bending of the film edges, bending of the inner sections of the film will be limited by contact between the neighboring sections of the film. Further lithiation is therefore required to generate sufficiently high tensile σ_{11} stresses to nucleate micro-cracks at a further inner distance d_c from the original crack sites. This sequential cracking mechanism is demonstrated in Fig. 12b for a h = 400 nm film with an initial island diameter of d = 20 μm. To model the micro-crack, a single 20 nm thick column of elements is removed at a distance d_c = 2.2 μm from the edges, and a contact algorithm is imposed between the crack surfaces. Lithiation of this silicon film shows that the free-surfaces created by the micro-crack allow the inner section of the film to bend; high tensile stresses in turn develop at a further distance d_c = 2.2 μm from the edges. This sequential cracking process is repeated until the constraints imposed by the contacting surfaces sufficiently limit bending and the development of high tensile stresses. Then, the cracking process is effectively terminated in the current lithiation cycle. During the next lithiation cycle, plastic deformation and ratcheting of the underlying copper substrate relaxes the constraints by the contacting surfaces (Maranchi et al., 2006), which allows the sequential cracking process to progress towards the center of the film. In this fashion, uniformly-spaced cracks are formed throughout the entire film after several lithiation and delithiation cycles.

The internal crack spacing d_c denotes the minimum possible diameter of the fractured islands. In reality, not all internal cracks

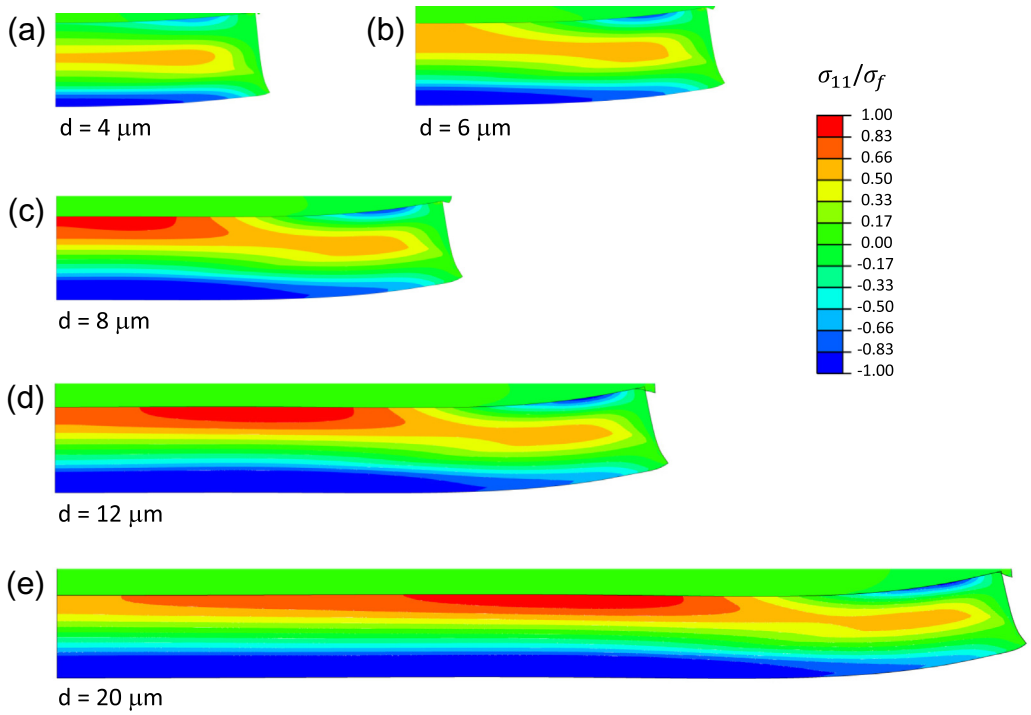

Fig. 11. Contour maps of σ_{11} stresses taken at the instant when the σ_{11} tensile stress within the silicon film reaches a maximum, for fixed film thickness of h = 800 nm, with d ranging from 4 μm to 20 μm.

can propagate to the surface. Our earlier simulations in Fig. 10 show that high internal tensile stresses, necessary for the propagation of the micro-cracks to the surface under repeated cycling, only develop within islands with diameters of approximately $2d_c$ and larger. Hence, while sequential internal cracks form at intervals of d_c from the edges, the typical silicon islands would have diameters of $2d_c$. To determine the actual island sizes, we iteratively vary d for each h to find the critical island diameter for which tensile stresses cannot build-up and fracture would be mitigated. We compared the predicted island sizes from our FEM simulations against available experimental data in Fig. 13 (Moon et al., 2006; Maranchi et al., 2006; Li et al., 2011). Our predicted island size matches the experimental results reasonably well across the entire range of film thicknesses considered ($300\text{ nm} \leqslant h \leqslant 1000\text{ nm}$). Note that in the experiments of Li et al. (2011), the substrate used is steel rather than copper. We have repeated our calculations using steel as a substrate material with $E_s = 200$ GPa and $\sigma_s = 0.25$ GPa, and have found the differences in the predicted island size d to be negligible for film thickness of $h \leqslant 600$ nm. For film thickness of $h = 800$ nm and larger, d is ~1–2 μm smaller with the steel substrate than with the copper substrate, due to higher interfacial stresses caused by the more rigid steel substrate. Our simulations predict a critical film thickness of $h = 200$ nm to mitigate fracture, which is larger than the critical thickness of $h = 100$ nm from experiments. This discrepancy is related to the charging and diffusion rates assumed in our simulations. We have shown that the development of the tensile stress zone depends significantly on the extent of lithiation in the film, and that the mitigation of fracture below a critical film thickness is a result of lithium diffusing to the copper/silicon interface; the associated volumetric expansion caused by the diffusion of lithium ions prevents large tensile stresses from building up. A slower charging rate J_0 or faster diffusion rate D_0 allows lithium ions to spread more uniformly throughout the film which would prevent high tensile stresses from developing during early-stage lithiation. On the other hand, a faster charging rate or slower diffusion rate would limit the spread of lithium ions, which would create distinct compression and tensile zones within the film. This could potentially explain why cracking is sometimes also observed even for amorphous silicon films with thickness of ~100 nm (Xiao et al., 2011; Nadimpalli et al., 2013). To further illustrate this point, we have repeated our simulations for the lithiation of silicon films using charging rates of $J_0 = 0.5$ and $2\text{ nm}^{-2}\text{ s}^{-1}$. The maximum tensile stresses σ_{11}^{max} are substantially higher for $J_0 = 2\text{ nm}^{-2}\text{ s}^{-1}$, and correspondingly lower for $J_0 = 0.5\text{ nm}^{-2}\text{ s}^{-1}$. Results of the σ_{11}^{max} for a fixed film diameter of $d = 4$ μm at different charging rates of $J_0 = 0.5$, 1, and $2\text{ nm}^{-2}\text{ s}^{-1}$ are summarized in Table 1. For a 200 nm thick film, increasing J_0 from 1 to $2\text{ nm}^{-2}\text{ s}^{-1}$ increases σ_{11}^{max} from 1.4 GPa to 1.8 GPa. Micro-cracks can now nucleate and grow in a 200 nm thick film, and the critical film thickness for fracture mitigation is now reduced to $h = 100$ nm which is in good agreement with experiments.

Experimental studies have shown that the yield strength of lithiated-silicon decreases slightly with increasing lithium concentration (Sethuraman et al., 2010). Our simulations show that the fracture process occurs during early-stage lithiation in the lithium-free silicon, where plasticity in the lithiated silicon is still confined to the surface of the film. Therefore our model assumption of lithium-concentration-independent yield strength will not significantly influence the above results. Evidence has also recently accumulated that in the lithiation of crystalline silicon, the rate limiting step is not in diffusion but in the chemical reaction between lithium and silicon (Chon et al., 2011; Zhao et al., 2012). This results in an atomically-sharp phase boundary between the crystalline silicon and the lithiated silicon, which would in turn create very well-delineated compressive and tensile sublayers. Based on the results of our simulations, we expect the effects of the size-dependent fracture seen in our diffusion-based model to be exacerbated in the case of the lithiation of crystalline silicon thin film electrodes.

Silicon films are known to fracture during lithiation and delithiation cycles, but an open question is whether the cracks initiate during lithiation or delithiation. Previous experiments appear to

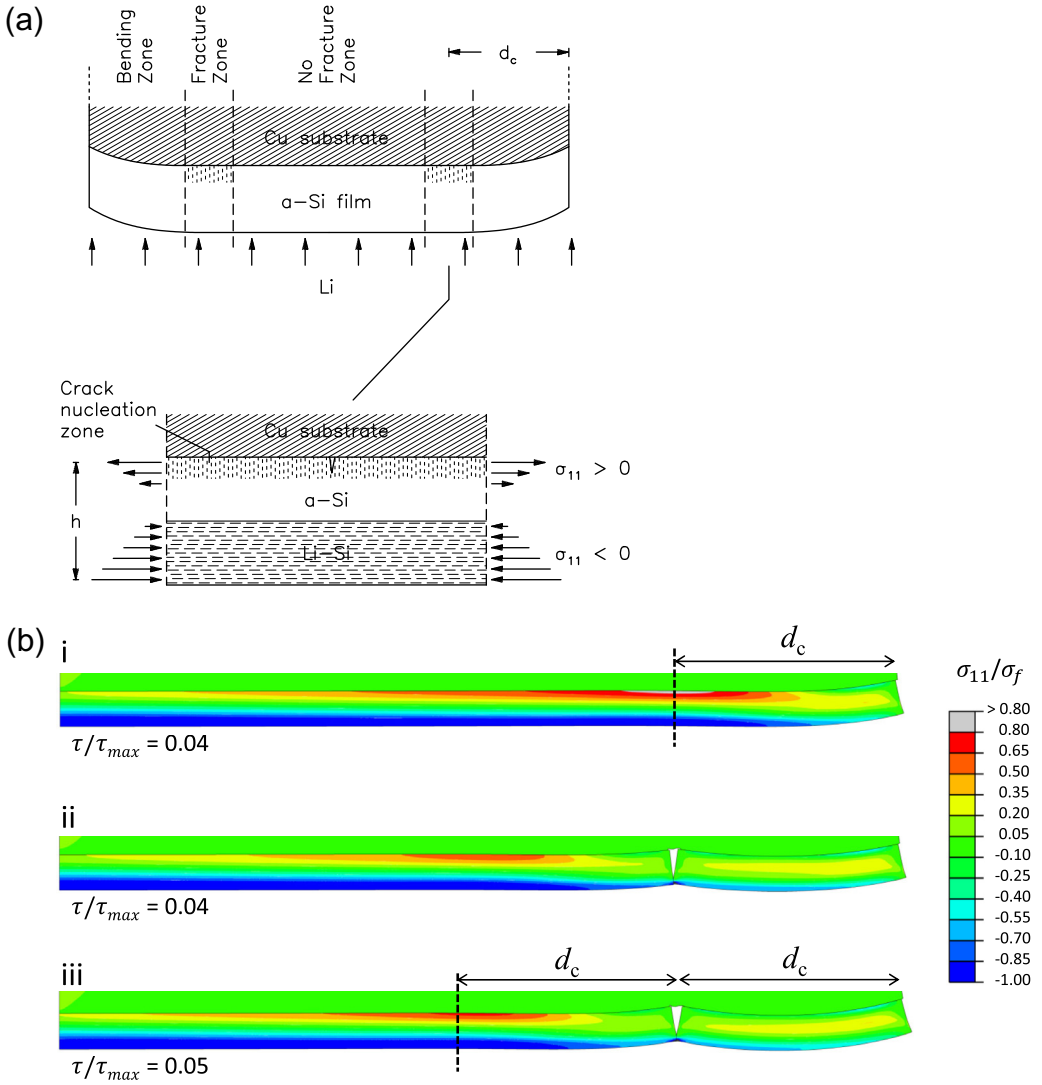

Fig. 12. Sequential cracking mechanism of the silicon thin film during early-stage lithiation resulting in multiple island formation. (a) Schematic showing the development of a high tensile stress zone caused by bending of the lithium-silicon subsurface layer near the film edges. A micro-crack develops in the high tension zone at a critical distance d_c from the edges. (b) Contour maps of σ_{11} stresses during sequential cracking. (i) Maximum σ_{11} tensile stress developing at d_c from the edges. (ii) Nucleation of a micro-crack which allows the inner sections of the film to bend. (iii) A new high σ_{11} tension zone develops at d_c from the crack after continued lithiation.

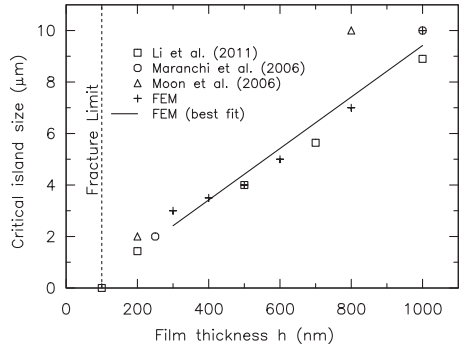

Fig. 13. Comparison of the critical island size for different film thickness h predicted by FEM simulations versus experiments.

Table 1
Maximum tensile stress σ_{11}^{max} versus film thickness h for silicon films with $d = 4$ μm subjected to different charging rates J_0.

Film thickness h (nm)	Maximum tensile stress σ_{11}^{max} (GPa)		
	$J_0 = 0.5$ nm^{-2} s^{-1}	$J_0 = 1$ nm^{-2} s^{-1}	$J_0 = 2$ nm^{-2} s^{-1}
100	0.50	0.86	1.24
200	0.92	1.36	1.82
300	1.21	1.68	2.14
400	1.39	1.87	1.82
500	1.46	1.51	1.36
600	1.01	1.09	1.46
800	0.75	1.18	1.50
1000	0.93	1.41	1.41

support the latter, with observations of surface cracks during delithiation (Li et al., 2011; Beaulieu et al., 2001). Our simulations instead point to the sequential nucleation of cracks within the lithium-free silicon during early-stage lithiation, from the edges to the center of the film. These internal cracks can only be observed from the surface of the film during delithiation, since the sub-surface of the film is under compression during lithiation. The formation of internal cracks during lithiation, however, does not rule out the possibility of surface cracks also nucleating during delithiation. To examine this possibility, we perform simulations for the delithiation of a $d = 4$ μm size, $h = 400$ nm thick silicon film which has an initial lithium concentration of $\bar{C} = 1$; a constant flux of

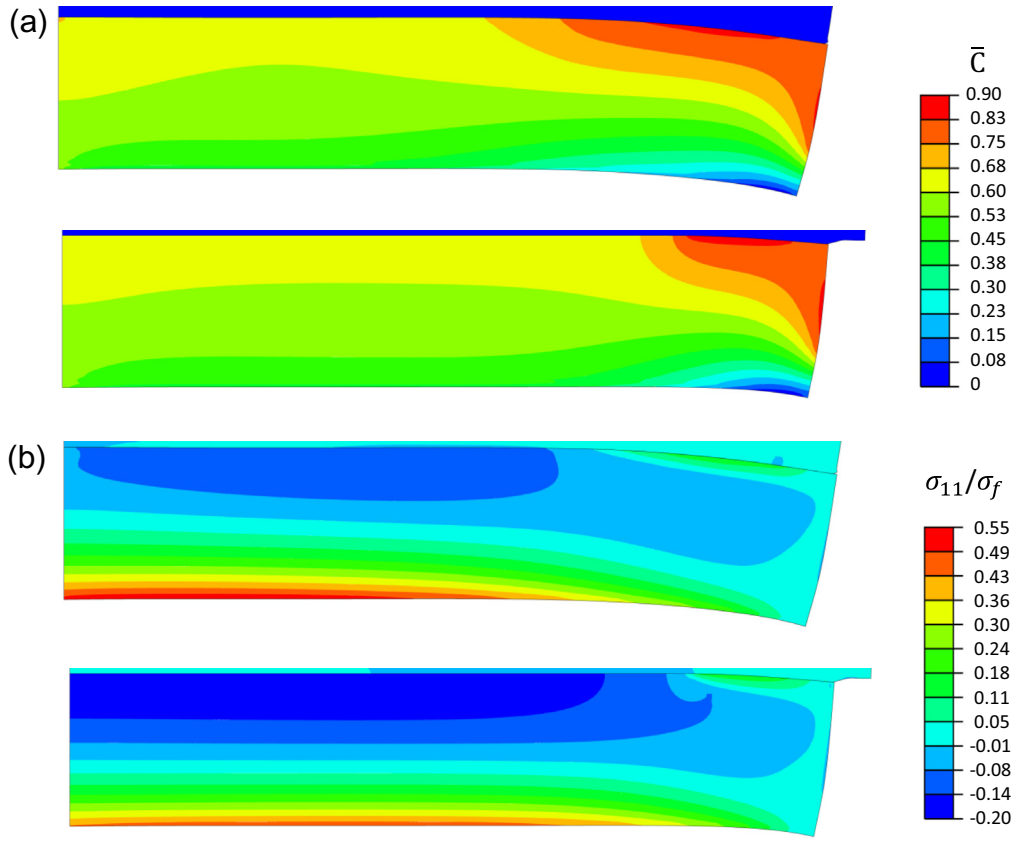

Fig. 14. Contour maps of normalized (a) lithium concentration $\bar{C}$ and (b) σ_{11} stresses in the film with $d = 4$ μm, $h = 400$ nm and an initial lithium concentration of $\bar{C} = 1$, subjected to delithiation with flux of $J_0 = -1$ nm^{-2}s^{-1}. No-slip boundary conditions are imposed along the film/substrate interface in the upper sub-plots, while interface slip is permitted for the lower sub-plots.

$J_0 = -1$ nm^{-2} s^{-1} is imposed at the surface of the film. Unlike the simulations for early-stage lithiation where the adhesion between the copper substrate and silicon film is strong, recent DFT calculations show that the accumulation of lithium ions near the film-substrate interface can lower the adhesion energy by an order of magnitude (Stournara et al., 2013). This reduced adhesion strength resulting in interface slip is also one of the main considerations in the theoretical argument of Xiao et al. (2011) to explain film cracking during the delithiation cycle. Here, we consider both the fully-bonded no-slip case, as well as the case where interface slip is permitted. For the latter, we assume a maximum shear stress of 0.211 GPa, which corresponds to the adhesion shear strength for $\bar{C} = 1$ measured from DFT calculations (Stournara et al., 2013). Fig. 14 shows the contour maps for lithium concentration $\bar{C}$ and σ_{11} stress in the film after steady-state lithium diffusion is attained. Observe that both the lithium concentration and σ_{11} stress distributions within the film are highly non-uniform, with tensile and compressive stress zones developing at regions of the film corresponding to low and high lithium concentrations respectively. The maximum tensile σ_{11} stress zone resides at the film surface and reaches $\sim$0.55 σ_f, which is several-folds lower than the tensile stress build-up associated with bending of the film edges during early-stage lithiation. We therefore conclude that cracking of the silicon film initiates during the lithiation process.

5. Conclusion

We have implemented a model for lithium diffusion in amorphous silicon thin films on copper substrates in the finite element method. The model fully accounts for the coupled effects of finite strains, plastic flow, and pressure-gradients on the diffusion of lithium. Our finite element results demonstrate that bending of the lithium-silicon subsurface layer near the film edges generates a high tensile stress zone at a fix distance away within the lithium-free silicon near the film/substrate interface during early-stage lithiation, which causes micro-cracks to develop. These micro-cracks in turn allow the inner film to bend, sequentially creating uniformly-spaced cracks from the edges of the film to the interior after repeated lithiation and delithiation cycles. The predicted silicon island sizes formed from these sequential micro-cracks are in excellent agreement with previous experiments across the range of film thickness considered. In addition, our simulations predict a critical film thickness of $\sim$100–200 nm below which the tensile stress zone diminishes and fracture would be mitigated, which is also in agreement with experiments. This sequential cracking mechanism is distinct from fracture induced by residual tension in conventional thin films. Knowledge of this cracking mechanism, as well as the critical island size and film thickness to mitigate electrode fracture, will directly impact the design and patterning of next generation silicon thin film batteries.

Acknowledgement

The supports of NSF grant nos. NSF-CMMI-1300805 and NSF-CMMI-1300458 are gratefully acknowledged.

References

Ballarini, R., Mullen, R.L., Yin, Y., Kahn, H., Stemmer, S., Heuer, A.H., 1997. The fracture toughness of polysilicon microdevices: a first report. J. Mater. Res. 12, 915–922.

Ballarini, R., Kahn, H., Tayebi, N., Heuer, A.H., 2001. Effects of microstructure on the strength and fracture toughness of polysilicon: a wafer level testing approach. In: Muhlstein, C.L., Brown, S.B. (Eds.), Mechanical Properties of Structural Films,

vol. STP 1413. American Society for Testing and Materials, Orlando, FL, pp. 37–51.
Beaulieu, L.Y., Eberman, K.W., Turner, R.L., Krause, L.J., Dahn, J.R., 2001. Colossal reversible volume changes in lithium alloys. Electrochem. Solid-State Lett. 4, A137–A140.
Bower, A.F., Guduru, P.R., Sethuraman, V.A., 2011. A finite strain model of stress, diffusion, plastic flow, and electrochemical reactions in a lithium-ion half-cell. J. Mech. Phys. Solids 59, 804–828.
Chasiotis, I., Cho, S.W., Jonnalagadda, K., 2005. Fracture toughness and subcritical crack growth in polycrystalline silicon. J. Appl. Mech. 73, 714–722.
Chen, C.P., Leipold, M.H., Helmreich, D., 1982. Fracture of directionally solidified multicrystalline silicon. J. Am. Chem. Soc. 65, C49.
Chon, M.J., Sethuraman, V.A., McCormick, A., Srinivasan, V., Guduru, P.R., 2011. Real-time measurement of stress and damage evolution during initial lithiation of crystalline silicon. Phys. Rev. Lett. 107, 045503.
Ding, N., Xu, J., Yao, Y.X., Wegner, G., Fang, X., Chen, C.H., Lieberwirth, I., 2009. Determination of the diffusion coefficient of lithium ions in nano-Si. Solid State Ionics 180, 222–225.
Goehring, L., Conroy, R., Akhter, A., Clegg, W.J., Routh, A.F., 2010. Evolution of mud-crack patterns during repeated drying cycles. Soft Matter 6, 3562–3567.
Graetz, J., Ahn, C.C., Yazami, R., Fultz, B., 2003. Highly reversible lithium storage in nanostructured silicon. Electrochem. Solid-State Lett. 6, A194–A197.
Huang, R., Prevost, J.H., Huang, Z.Y., Suo, Z., 2003. Channel-cracking of thin films with the extended finite element method. Eng. Fract. Mech. 70, 2513–2526.
Huang, S., Fan, F., Li, J., Zhang, S., Zhu, T., 2013. Stress generation during lithiation of high-capacity electrode particles in lithium ion batteries. Acta. Mater. 61, 4354–4364.
Lee, S.W., McDowell, M.T., Beria, L.A., Nix, W.D., Cui, Y., 2012. Fracture of crystalline silicon nanopillars during electrochemical lithium insertion. PNAS 109, 4080–4085.
Li, J., Dozier, A.K., Li, Y., Yang, F., Cheng, Y.-T., 2011. Crack pattern formation in thin film lithium-ion battery electrodes. J. Electrochem. Soc. 158, A689–A694.
Liu, X.H., Zheng, H., Zhong, L., Huang, S., Karki, K., Zhang, L.Q., Liu, Y., Kushima, A., Liang, W.T., Wang, J.W., Cho, J.-H., Epstein, E., Sayeh, S.A., Picraux, S.T., Zhu, T., Li, J., Sullivan, J.P., Cumings, J., Wang, C., Mao, S.X., Ye, Z.Z., Zhang, S., Huang, J.Y., 2011. Anisotropic swelling and fracture of silicon nanowires during lithiation. Nano Lett. 11, 3312–3318.
Liu, X.H., Zhong, L., Huang, S., Mao, S.X., Zhu, T., Huang, J.Y., 2012. Size-dependent fracture of silicon nanoparticles during lithiation. ACS Nano 6, 1522–1531.
Maranchi, J.P., Hepp, A.F., Evans, A.G., Nuhfer, N.T., Kumta, P.N., 2006. Interfacial properties of the a-Si/Cu: active-inactive thin-film anode system for lithium-ion batteries. J. Electrochem. Soc. 153, A1246–A1253.
Mohr, P.J., Taylor, B.N., Newell, D.B., 2008. CODATA recommended values of the fundamental physical constants: 2006. Rev. Mod. Phys. 80, 633–730.
Moon, T., Kim, C., Park, B., 2006. Electrochemical performance of amorphous-silicon thin films for lithium rechargeable batteries. J. Power Sources 155, 391–394.
Nadimpalli, S.P.V., Sethuraman, V.A., Bucci, G., Srinivasan, V., Bower, A.F., Guduru, P.R., 2013. On plastic deformation and fracture in Si films during electrochemical lithiation/delithiation cycling. J. Electrochem. Soc. 160, A1885–A1893.
Pharr, M., Suo, Z., Vlassak, J.J., 2013. Measurements of the fracture energy of lithiated silicon electrodes of Li-ion batteries. Nano Lett. 13, 5570–5577.
Ryu, I., Choi, J.W., Cui, Y., Nix, W.D., 2011. Size-dependent fracture of Si nanowire battery anodes. J. Mech. Phys. Solids 59, 1717–1730.
Sethuraman, V.A., Srinivasan, V., Bower, A.F., Guduru, P.R., 2010. In situ measurement of stress-potential coupling in lithiated silicon. J. Electrochem. Soc. Commun. 12, 1614–1617.
Shenoy, V.B., Johari, P., Qi, Y., 2010. Elastic softening of amorphous and crystalline Li–Si phases with increasing Li concentration: a first-principles study. J. Power Sources 195, 6825–6830.
Stournara, M., Xiao, X., Qi, Y., Johari, P.S., Lu, P., Sheldon, B.W., Gao, H., Shenoy, V.B., 2013. Li segregation induces structure and strength changes at the amorphous Si/Cu interface. Nano Lett. 13, 4759–4768.
Takamura, T., Ohara, S., Uehara, M., Suzuki, J., Sekine, K., 2004. A vacuum deposited Si film having a Li extraction capacity over 2000 mAh/g with a long cycle life. J. Power Sources 129, 96–100.
Xia, Z.C., Hutchinson, J.W., 2000. Crack patterns in thin films. J. Mech. Phys. Solids 48, 1107–1131.
Xiao, X., Liu, P., Verbrugge, M.W., Haftbaradaran, H., Gao, H., 2011. Improved cycling stability of silicon thin film electrodes through patterning for high energy density lithium batteries. J. Power Sources 196, 1409–1416.
Ye, T., Suo, Z., Evans, A.G., 1992. Thin film cracking and the roles of substrate and interface. Int. J. Solids Struct. 29, 2639–2648.
Zhao, K., Pharr, M., Cai, S., Vlassak, J.J., Suo, Z., 2011. Large plastic deformation in high-capacity lithium-ion batteries caused by charge and discharge. J. Am. Ceram. Soc. 94, S226–S235.
Zhao, K., Pharr, M., Wan, Q., Wang, W.L., Kaxiras, E., Vlassak, J.J., Suo, Z., 2012. Concurrent reaction and plasticity during initial lithiation of crystalline silicon in lithium-ion batteries. J. Electrochem. Soc. 159, A238–A243.